Determination of fatty acid methyl esters by two-color two-photon resonance-enhanced femtosecond ionization mass spectrometry

Yoshinaga, Katsunori
Faculty of Design, Kyushu University

Wen, Lu
Faculty of Design, Kyushu University

Imasaka, Totaro
Kyushu University

Imasaka, Tomoko
Faculty of Design, Kyushu University

出版情報：Analytica Chimica Acta. 1296, pp.342341-, 2024-04-01. Elsevier
バージョン：

Determination of fatty acid methyl esters by two-color two-photon resonance-enhanced femtosecond ionization mass spectrometry

Katsunori Yoshinaga,[a,1] Lu Wen,[a,1,2] Totaro Imasaka,[b,c] and Tomoko Imasaka[a]*

[a]*Faculty of Design, Kyushu University, 4-9-1, Shiobaru, Minami-ku, Fukuoka 815-8540: 744 Motooka, Nishi-ku, Fukuoka 819-0395, Japan*

[b]*Kyushu University, 744 Motooka, Nishi-ku, Fukuoka 819-0395, Japan*

[c]*Hikari Giken, Co., 2-10-30, Sakurazaka, Chuou-ku, Fukuoka 810-0024, Japan*

* Corresponding author.

Email address: imasaka@design.kyushu-u.ac.jp (Tomoko Imasaka).

1. These authors have contributed equally to this work.

2. Present address: Shijiazhuang University, No.288, Zhufeng street, Shijiazhuang high tech Development Zone, China.

ABSTRACT

A standard sample mixture containing thirty-seven fatty acid methyl esters (FAMEs) was measured by femtosecond laser ionization mass spectrometry. FAME molecules with double bonds were efficiently ionized via resonance-enhanced two-photon ionization by absorbing the first photon at 206 nm at the edge of the absorption band of the $\pi \rightarrow \pi^*$ transition and subsequently ionized by absorbing the second photon at 257 nm. The intensity of the molecular radical ion was enhanced significantly using this two-color ionization scheme, which minimizes the excess energy in the ionized state, when compared with electron ionization mass spectrometry and vacuum-ultraviolet photoionization mass spectrometry. This approach was then used for the reliable identification of FAMEs contained in an actual sample of biofuel.

Keywords: femtosecond ionization, mass spectrometry, molecular radical ion, fatty acid methyl ester, biofuel

1. Introduction

The level of the carbon dioxide in the atmosphere has increased more rapidly since the beginning of the 20th century and has resulted in serious global warming. For the survival of humans and all other organisms on earth, this issue needs to be solved urgently. One solution to this problem is the use of biofuel to minimize the rate of consumption of fossil fuel. A variety of feedstocks have been studied for use as biofuels. Oleaginous compounds such as glycerides that are made up of fatty acids are converted into fatty acid methyl esters (FAMEs) by a transesterification reaction [1,2]. The product of FAMEs is then utilized directly as a diesel fuel (B100) or after mixing it with kerosene (B5 for a mixture of 5% FAMEs and 95% kerosene). The properties of the biofuel being used affect the performance of a diesel engine [3], and therefore, values such as a cetane number, cold flow point, and oxidative stability need to be evaluated prior to their use [4-8]. These properties are strongly dependent on the FAME composition of the material. For example, a biofuel containing unsaturated FAMEs would have a cold filter plugging point, permitting its use in cold countries. On the other hand, such the biofuel is potentially more oxidative and would lead to serious damage to the diesel engine [6]. Accordingly, it is necessary to measure the FAMEs in the biofuel and to evaluate the properties of the fuel prior to use.

There are two types of approaches for the evaluation of biofuels. One is the direct measurement of physical parameters such as the cetane number of the biofuel [2,4]. This approach is practically useful for characterizing a biofuel. However, many other parameters need to be measured, which is time-consuming and requires special skills. For example, it takes 1-17 h for measuring oxidative stability, and the reproducibility was rather poor even in the repeated measurements [9,10]. The other is the measurement of the constituents of the FAMEs in the biofuel, since the properties of the fuel can be predicted from the contents of the FAMEs [6,11,12]. Since there are many types of FAMEs with similar chemical structures having different chain lengths and different numbers of double bonds, they need to be separated by a technique such as gas chromatography (GC) combined with a flame ionization detector (FID) [13,14] or a vacuum-ultraviolet (VUV) absorption detector [15]. Mass spectrometry (MS) can be easily combined with GC, thus leading to higher sensitivity and selectivity [16,17]. For better separation resolution of GC, the length of the capillary column has been extended to 100 m, permitting the determination of 139 FAMEs in a biofuel [14,18]. On the other hand, the use of a short column (4 and 5.5 m) results in a decreased separation time [19,20]. The optimal stationary phase of the column was studied in order to achieve a better separation resolution of the FAMEs, suggesting the use of a capillary column with low polarity (OV1) [21]. Comprehensive two-

dimensional GC, referred to as GC × GC, combined with FID or time-of-flight MS (TOFMS), frequently results in superior separation [22,23]. A flame-induced atmospheric pressure chemical ionization source has been developed for use in a combination of GC and MS [24]. As reported previously, MS is a superior technique for measuring the FAMEs. However, the molecules easily dissociate to produce many fragments through the McLafferty rearrangement and subsequent fragmentation, in which a hydrogen atom combined with the carbon atom located at the γ-position dissociates in the first step to combine with a carbonyl group and then numerous fragment ions appear by the cleavage of the carbon-carbon bond in a mass-charge ratio (*m/z*) of <150 (major peaks appear at around *m/z* = 74 and 87). These undesirable signals make the reliable identification of FAMEs more difficult. Therefore, developing a soft ionization technique for the reliable determination of the FAMEs in a real biofuel sample would be highly desirable.

Photoionization is a well-known technique for soft ionization, which permits a molecular radical ion to be observed in many cases [25]. In fact, FAMEs have been successfully measured by MS using a deuterium lamp (10.8 eV) as a single-photon ionization source. For example, a molecular radical ion was observed for large FAME molecules such as C20:3 (the number of carbon atoms in the side chain is 20 and the number of double bonds is 3), although molecular radical ions are not produced for C20:4 and C20:5 [26]. When an ultraviolet (UV) laser is used for two-photon ionization, the first photon can be used for excitation and the second photon for subsequent ionization. A nanosecond laser with a narrow spectral bandwidth can be used successfully for the selective ionization of aromatic hydrocarbons. It is, however, difficult to apply this technique to compounds with short excited-state lifetimes. In contrast, a femtosecond laser is useful for efficient ionization even for non-aromatic hydrocarbons [27-29], in which the excess energy remaining in the ionic state can be zero by adjusting the laser wavelength to half of the ionization energy. Accordingly, a molecular radical ion can be observed in most cases by optimizing the laser wavelength [30,31]. In fact, a recent study reported that the intensity of a molecular radical ion can be enhanced significantly for nitrated polycyclic aromatic hydrocarbons with femtosecond lifetimes using the femtosecond optical pulses emitting in the near-ultraviolet (343 nm) and ultraviolet (257 nm) regions [32].

In this study, we report on the determination of FAMEs in a biofuel. The absorption band arising from the allowed π-π* transition appears at the edge of the deep-ultraviolet (DUV) region for unsaturated compounds [15]. On the other hand, the absorption band arising from the forbidden n-π* transition appears in the DUV region, even for saturated compounds. The FAME molecule was then excited at 206 nm through the π-π* transition for unsaturated compounds and through the n-π* transition for saturated compounds and subsequently ionized at 257 nm to minimize the excess energy

in the ionic state, in order to enhance the molecular radical ion for the reliable identification of FAMEs in a complicated matrix. This technique based on two-color two-photon femtosecond ionization was employed for measuring a standard sample mixture containing 37 FAMEs and also FAMEs in a real biofuel sample.

2. Experimental section

2.1. Samples

A sample mixture containing 37 FAMEs, which was supplied by Spelco, Japan (CRM18919, Product No. 18919-1AMP), contains 1 methyl butyrate (C4:0), 2 methyl hexanoate (C6:0), 3 methyl octanoate (C8:0), 4 methyl decanoate (C10:0), 5 methyl undecanoate (C11:0), 6 methyl laurate (C12:0), 7 methyl tridecanoate (C13:0), 8 methyl myristoleate (C14:1), 9 methyl myristate (C14:0), 10 methyl *cis*-10-pentadecenoate (C15:1), 11 methyl pentadecanoate (C15:0), 12 methyl palmitoleate (C16:1), 13 methyl palmitate (C16:0), 14 methyl *cis*-10-heptadecenoate (C17:1), 15 methyl heptadecanoate (C17:0), 16 methyl gamma-linolenate (C18:3), 17 methyl linolenate (C18:3), 18 methyl linoleate (C18:2), 19 methyl linolelaidate (C18:2), 20 methyl oleate (C18:1), 21 methyl elaidate (C18:1), 22 methyl stearate (C18:0), 23 methyl *cis*-5,8,11,14,17-eicosapentaenoate (C20:5), 24 methyl *cis*-5,8,11,14-eicosatetraenoate (C20:4), 25 methyl *cis*-8,11,14-eicosatrienoate (C20:3), 26 methyl *cis*-11,14,17-eicosatrienoate (C20:3), 27 methyl *cis*-11,14-eicosadienoate (C20:2), 28 methyl *cis*-11-eicosenoate (C20:1), 29 methyl arachidate (C20:0), 30 methyl heneicosanoate (C21:0), 31 methyl *cis*-4,7,10,13,16,19-docosahexaenoate (C22:6), 32 methyl *cis*-13,16-docosadienoate (C22:2), 33 methyl erucate (C22:1), 34 methyl behenate (C22:0), 35 methyl tricosanoate (C23:0), 36 methyl nervonate (C24:1), and 37 methyl lignocerate (C24:0). The chemical structures for C18:0 - C18:3 are shown in Fig. 1. The chemical structures for all the FAMEs used in this study are shown in Fig. S1 in the Supplementary Information. The concentrations of FAMEs are indicated in Fig. S2. Note that a reference material of CRM18918 containing 14 FAMES was also measured and the results were used for assigning the FAME signals in GC-MS. An actual sample of B5 (a biofuel diluted to 5% with kerosene) was obtained from Revo International Co., Ltd, a company that processes waste cooking oils. The sample was stored in a refrigerator and was diluted stepwise with dichloromethane prior to the measurements.

2.2. Analytical instrument

Fig. 2 shows the experimental apparatus used in this study. The operation principle, the performance, and the experimental conditions have been reported in detail elsewhere [33]. Briefly, a sample mixture containing FAMEs (1 μL) was injected into a GC (6890N, Agilent Technologies) and was separated with a DB-5ms capillary column (length 30 m, inner diameter 0.25 mm, film thickness 0.25 μm, Agilent Technologies). The temperature program for the GC column was as follows; the initial temperature of the column was held at 50 ºC for 4 min, a ramp of 30 ºC/min to 160 ºC and held for 3 min, then an increase to 240 ºC by 10 ºC/min rate and a 2 min hold, and finally a ramp of 5 ºC/min to 300 ºC. Helium was used as a carrier gas at a flow rate of 1 mL/min. The temperatures of the sample injection port and the transfer line between the GC to the MS were maintained at 280 and 300 ºC, respectively. The analytes eluting from the GC column was measured by femtosecond laser ionization mass spectrometry (fsLIMS) consisting of a small-frame TOF mass analyzer developed in this laboratory and is now commercially available (HG-2, Hikari Giken). The signal from a microchannel detector (F4655-11, Hamamatsu Photonics) was passed through an amplifier (C5594, bandwidth 1.5 GHz, Hamamatsu Photonics). The time interval between the electronic pulses from the laser (start pulse) and the amplifier (stop pulse) was measured using a time-to-digital converter (TimeHarp 260 NANO, PicoQuant). A histogram was constructed by accumulating the signals and was displayed on a monitor using a software program developed in this laboratory.

2.3. Computational method

Spectroscopic parameters such as the lowest excitation energy (*EE*) and the ionization energy (*IE*) were calculated for neutral and ionic states by the Gaussian 16 program series package. The minimum geometries were obtained by the ωB97XD method, based on density functional theory (DFT) with a cc-pVDZ basis set [34]. A vertical ionization energy was calculated from the difference between the energies obtained at the level of ωB97XD/cc-pVTZ of the ground and ionic states. The lowest one-hundred singlet transition energies and the oscillator strengths were calculated using time-dependent DFT (TD-DFT) at the ωB97XD/cc-pVTZ level. The absorption spectra were then constructed using the GaussView 6 software program. The energy levels related to n- and π-orbitals for the highest occupied molecular orbital (HOMO) and the lowest unoccupied molecular orbital (LUMO) were recognized from the shape of the molecular orbitals.

3. Results and discussion

3.1. Spectral properties

The absorption spectra of the neutral and ionic species for stearic, oleic, linoleic, and linolenic methyl esters (C18:0, C18:1, C18:2, C18:3) were calculated (the data are shown in Fig. S2). A saturated compound such as stearic acid methyl ester had a small absorption band based on a forbidden n-π* transition with a molar absorptivity of ca. 50 at around 210 nm and large absorption bands based on an allowed π-π* transition with an absorptivity of ~10^4 at 130 and 160 nm. The threshold for two-photon ionization (*IE*/2) was located at around 300 nm. Note that the ionic state has a considerably large absorption band at around 200 nm, suggesting subsequent photodissociation from the ionic state by absorbing an additional photon at around 206 nm. The absorption band was shifted to longer wavelengths, reaching 200 nm at the edge for a mono-unsaturated compound such as C18:1. For poly-unsaturated FAMEs such as C18:2 and C18:3, another absorption band appeared at around 200 nm, allowing more efficient excitation at 206 nm. These calculated data are supported by the VUV-DUV absorption spectra reported for the FAME molecules [15].

The ionization scheme of FAMEs is summarized in Fig. 3. An unsaturated FAME molecule can be excited from the π state (C=C) as shown in Fig. 3(A) and then be ionized using two photons of the fifth harmonic emission at 206 nm via the π* state (C=C) (12.0 eV). However, the excess energy increases significantly when single-color two-photon ionization is used. In contrast, the fourth harmonic emission at 257 nm can be used for non-resonant two-photon ionization (9.64 eV) (the data of *EE* and *IE* calculated are listed in Table S1). However, this scheme results in less efficient ionization due to the non-resonant process. Accordingly, the molecule should be excited at 206 nm and subsequently ionized at 257 nm. This approach, referred to as resonance-enhanced two-color two-photon ionization, is useful for decreasing the excess energy in the ionic state, thus allowing a molecular radical ion to be observed. This benefit becomes more important for poly-unsaturated FAMEs, since another peak appears at around 200 nm. On the other hand, a saturated FAME molecule can be excited from the n-state (C=O) and be ionized via the π* state (C=O) as shown in Fig. 3 (B). Since this is a forbidden n-π* process and is less efficient than the process shown in Fig. 3 (A). A similar ionization scheme (n-π*) is possible for unsaturated compounds. However, such a transition would be hidden by the π-π* transition arising from the C=C bond because of the small oscillator strengths for the transition arising from a C=O bond.

3.2. Two-dimensional display

A two-dimensional display of the GC-MS data measured using a two-color two-photon ionization scheme (206 + 257 nm) is shown in Fig. 4(A) (the two-dimensional displays measured at

257 and 206 nm are shown in Figs. S3(A) and (B), respectively). The retention time (t_r) of the FAME molecule increased regularly with the molecular weight when a nearly non-polar (or slightly polar) DB5-ms column was used. It should be noted that the signals corresponding to molecular radical ions are clearly observed for all the FAMEs. Expanded views of the portions, where C18:0 - C18:3, C20:0 - C20:5, and C22:0 - C22:6 appear, are shown in Fig. 4(B). As demonstrated, all 37 FAMEs could be separated by the conventional DB5-ms column and were identified by fsLIMS. Compounds with larger numbers of double bonds (i.e., smaller molecular weights) and the *cis*-isomer eluted earlier from the DB5-ms column. It is interesting to note that methyl gamma-linolenate (16, C18:3n6, *cis*) appears earlier than methyl linolenate (17, C18:3n3, *cis*) (see Fig. 1 for the chemical structures). Therefore, the signal peak that appeared earlier for C:20:3 at m/z = 320 was tentatively assigned to methyl *cis*-8,11,14-eicosatrienoate (25, C20:3n6) rather than methyl *cis*-11,14,17-eicosatrienoate (26, C20:3n3). The signal intensity of the molecular radical ion was significantly enhanced for mono- and more for poly-unsaturated FAMEs.

3.3. Mass spectra

The mass spectra observed for several FAMEs are shown in Fig. 5 (data for C18:0 - C18:3, C20:0 - C20:5, and C22:0 - C22:6 are shown in Fig. S4). Molecular radical ions were clearly observed for all of the FAMEs in fsLIMS. This result is in contrast to data obtained by electron ionization mass spectrometry (EIMS) [24,26], in which fragmentation was dominant and a molecular radical ion was not observed for large poly-unsaturated FAMEs. The fragment patterns observed in fsLIMS were very similar to those observed in VUV photoionization mass spectrometry (PIMS) [26]. However, molecular radical ions were clearly observed even for highly poly-unsaturated FAMEs such as C20:5 and C22:6 in fsLIMS. The signal intensity of the unsaturated FAME was enhanced, which can be explained by efficient resonance-enhanced two-photon ionization (see Fig. 3). Accordingly, this technique would be useful for the determination of highly poly-unsaturated FAMEs in a complex matrix sample. However, the signal intensity decreases with increasing molecular weight and increasing number of the double bonds in a molecule. This unfavorable effect can be attributed to a decrease in ionization energy for large FAME molecules (e.g., 8.42 eV for C22:6), increasing the excess energy in the ionic state and accelerating the dissociation. In order to avoid this undesirable effect, the use of a different two-color two-photon ionization scheme is suggested. For example, a combination of the fifth (206 nm) and third harmonic emissions (343 nm), the total photon energy being 9.64 eV, would be beneficial (see Fig. 3(A)), although saturated FAMEs (e.g., *IE* = 9.92 eV for C18:0) are difficult to be ionized using these two photons.

3.4. Enhancement of molecular radical ion

The ratios of the signal intensities for the molecular and fragment ions measured for a series of C20:0 - C20:5 by fsLIMS, EIMS, and PIMS are summarized in Table 1 (data for all of the FAMEs are summarized in Table S2). The values were 0.32 - 11.9 for fsLIMS, which was significantly larger than the values reported by EIMS (<0.005 - 0.41) and PIMS (<0.005 - 2.1). These data suggest that fsLIMS has a distinct advantage over EIMS (6.6 - 340) and PIMS (1.3 - >64) in terms of observing a molecular radical ion. Note that fsLIMS is superior to PIMS even though it has a larger total photon energy (10.96 eV) than PIMS (10.8 eV). This unexpected result would be explained by the efficient relaxation to lower levels in the excited state before subsequent absorption of the second photon [32], thus decreasing the excess energy in the ionic state. The signal enhancement achieved by fsLIMS was more distinctive for highly poly-unsaturated FAMEs. Thus, the present technique would be useful for the analysis of trace levels of essential fatty acids such as eicosapentaenoic acid (EPA, C20:5) and docosahexaenoic acid (DHA, C22:6) in food science as well (see the data shown in Fig. S4(4)) [35].

3.5. Real sample

A two-dimensional display of GC-MS was measured for an actual sample of B5 to demonstrate the advantage of fsLIMS. The total view and the expanded view where C18:0 - C18:3 appear are shown in Figs. 6(A) and (B), respectively. The concentration distribution of the FAMEs in B5 (C18:1(20):C18:2(18):C18:3(17)) was 53:40:7 (note: the value for C18:1(20) is slightly underestimated by an overlap of the signal with C18:2(19) in Fig. 4(B)) and was similar to the values reported for canola (66:23:11) and rapeseed (66:24:9) [6], suggesting that the feedstock was a waste cooking oil [36,37]. The present data indicate that methyl linolelaidate (C18:2, No.19), the *trans* form of methyl linoleate (C18:2, No.18), is seldom observed in the natural product. Large background signals appeared probably from the fragment ions derived from the saturated aliphatic hydrocarbons of kerosene via non-resonant two-photon ionization, because of similar ionization energies (ca. 10 eV) [38]. However, a molecular radical ion was observed at *m/z* values larger than those for the fragment ions from saturated aliphatic hydrocarbons. Thus, the signals for the FAMEs were isolated from the background signals. The limit of detection (S/N = 3), the limit of quantification (S/N = 10), and the dynamic range were calculated for the signal of methyl linoleate (No. 18) to be 3, 11, and 0-1000 ppm, respectively. It would be possible to further decrease the background signal arising from aliphatic hydrocarbons by using a pump-and-probe technique (time-delayed measurement) to suppress the non-resonant two-photon ionization.

4. Conclusion

A two-color two-photon ionization scheme was employed for measuring FAMEs, in which the first photon emitting at 206 nm was used for a π-π* transition of the electron localized at the C=C bond for unsaturated FAMEs and a n-π* transition of the electron at the C=O bond for saturated FAMEs, followed by the second photon emitting at 257 nm for subsequent ionization. This approach based on fsLIMS was useful for increasing signal intensity of the molecular radical ion by resonance-enhanced two-photon ionization and for decreasing the excess energy in the ionic state, thus permitting the observation of a molecular radical ion. As a result, an actual sample (B5), a mixture of 5% FAMEs with 95% kerosene, was determined without pretreatment on the two-dimensional display of GC-MS, providing information concerning the concentrations of the FAMEs and also the type of feedstock utilized for the biofuel.

CRediT authorship contribution statement

Katsunori Yoshinaga: Measured the standard and real samples reported in the manuscript. **Lu Wen:** Measured the standard sample containing FAMEs. **Totaro Imasaka:** Supervised the research and wrote the original draft of this paper. **Tomoko Imasaka:** Funding acquisition, supervision, computational calculations, and revision of the draft.

Declaration of competing interest

The authors declare no competing financial interest.

Acknowledgments

This research was supported by the AMADA Foundation and the Murata Science Foundation. Quantum chemical calculations were mainly carried out using the computer facilities at the Research Institute for Information Technology, Kyushu University.

Appendix A. Supplementary data

Supplementary data to this article can be found online at ……

References

[1] L. C. Meher, D. V. Sagar, S. N. Naik, Technical aspects of biodiesel production by transesterification – A review. Renewable Sustainable Energy Rev. 10 (2006) 248-268.

[2] D. Y. C. Leung, X. Wu, M. K. H. Leung, A review on biodiesel production using catalyzed transesterification. Appl. Energy 87 (2010) 1083-1095.

[3] A. K. Agarwal, Biofuels (alcohols and biodiesel) applications as fuels for internal combustion engines. Prog. Energy Combust. Sci. 33 (2007) 233-271.

[4] M. S. Graboski, R. L. McCormick, Combustion of fat and vegetable oil derived fuels in diesel engines. Prog. Energy Combust. Sci. 24 (1998) 125-164.

[5] G. Knothe, Dependence of biodiesel fuel properties on the structure of fatty acid alkyl esters. Fuel Process. Technol. 86 (2005) 1059-1070.

[6] S. K. Hoekman, A. Broch, C. Robbins, E. Ceniceros, M. Natarajan, Review of biodiesel composition, properties, and specifications. Renewable Sustainable Energy Rev. 16 (2012) 143-169.

[7] G. Knothe, L. F. Razon, Biodiesel fuels. Prog. Energy Combust. Sci. 58 (2017) 36-59.

[8] D. Singh, D. Sharma, S. L. Soni, S. Sharma, D. Kumari, Chemical compositions, properties, and standards for different generation biodiesels: A review. Fuel 253 (2019) 60-71.

[9] C. Besser, L. Pisarova, M. Frauscher, H. Hunger, U. Litzow, A. Orfaniotis, N. Dörr, Oxidation products of biodiesel in diesel fuel generated by artificial alteration and identified by mass spectrometry. Fuel 206 (2017) 524-533.

[10] J. Pullen, K. Saeed, An overview of biodiesel oxidation stability. Renewable Sustainable Energy Rev. 16 (2012) 5924-5950.

[11] G. Kongprawes, D. Wongsawaeng, P. Hosemann, K. Ngaosuwan, W. Kiatkittipong, S. Assabumrungrat, Improvement of oxidation stability of fatty acid methyl esters derived from soybean oil via partially hydrogeneration using dielectric barrier discharge plasma. Int. J. Energy Res. 45 (2021) 4519-4533.

[12] L. F. Ramírez-Verduzco, J. E. Rodríguez-Rodríguez, A. R. Jaramillo-Jacob, Predicting cetane number, kinematic viscosity, density and higher heating value of biodiesel from its fatty acid methyl ester composition. Fuel 91 (2012) 102-111.

[13] Sahar, S. Sadaf, J. Iqbal, I. Ullah, H. N. Bhatti, S. Nouren, Habib-ur-Rehman, J. Nisar, M. Iqbal, Biodiesel production from waster cooking oil: An efficient technique to convert waste into biodiesel. Sustainable Cities and Society 41 (2018) 220-226.

[14] R. S. Gravador, A. G. Fahey, S. M. Harrison, V. Gkarane, A. P. Moloney, N. P. Brunton, N. A. Claffey, M. G. Diskin, L. J. Farmer, P. Allen, F. J. Monahan, Effects of silage to concentrate ratio and duration of feeding on the fatty acid composition of ovine muscle and adipose tissue. Anim. Prod. Sci. 62 (2022) 682-690.

[15] H. Fan, J. Smuts, L. Bai, P. Walsh, D. W. Armstrong, K. A. Schug, Gas chromatography - vacuum ultraviolet spectroscopy for analysis of fatty acid methyl esters. Food Chem. 194 (2016) 265-271.

[16] Z. Shuping, W. Yulong, Y. Mingde, I. Kaleem, L. Chun, Production and characterization of bio-oil from hydrothermal liquefaction of microalgae *Dunaliella tertiolecta* cake. J. Tong, Energy 35 (2010) 5406-5411.

[17] C. Besser, L. Pisarova, M. Frauscher, H. Hunger, U. Litzow, A. Orfaniotis, N. Dörr, Oxidation products of biodiesel in diesel fuel generated by artificial alteration and identified by mass spectrometry. Fuel 206 (2017) 524-533.

[18] Y. Abe, M. Toba, T. Mochizuki, Y. Yoshimura, Oxidative degradation behavior of fatty acid methyl ester in fish oil biodiesel and improvement of oxidation stability by partial hydrogenation. J. Jpn. Petrol. Inst. 52 (2009) 307-315.

[19] K. Ramos, A. Riddell, H. Tsiagras, A. M. Hupp, Analysis of biodiesel-diesel blends: Does ultrafast gas chromatography provide for similar separation in a fraction of the time? J. Chromatogr. A 1667 (2022) 462903.

[20] R. C. Blase, M. J. Libardoni, G. P. Miller, K. E. Miller, C. M. Phillips-Lander, C. R. Glein, J. H. Waite, A. Ghosh, A. Venkatasubramanian, M. W. Li, A. Stephens, X. Fan, K. Kurabayashi, MEMS GC column performance for analyzing organics and biological molecules for future landed planetary missions. Front. Astron. Space Sci. 9 (2022) 828103.

[21] N. E. Al-Beloshi, H. Al-Awadhi, R. A. Al-Khalaf, J. Jacquilion, S. Oommen, M. Afzal, Optimization of bacterial fatty acid methyl esters separation by gas chromatography - mass spectrometry. Kuwait J. Sci. Eng. 39 (2012) 159-168.

[22] P. Manzano, E. Arnáiz, J. C. Diego, L. Toribio, C. García-Viguera, J. L. Bernal, J. Bernal, Comprehensive two-dimensional gas chromatography with capillary flow modulation to separate FAME isomers. J. Chromatogr. A 1218 (2011) 4952-4959.

[23] M. Galletta, M. Zoccali, N. Jones, L. Mondello, P. Q. Tranchida, Flow-modulated comprehensive two-dimensional gas chromatography combined with time-of-flight mass spectrometry: Use of hydrogen as a more sustainable alternative to helium. Anal. Bioanal. Chem. 414 (2022) 6371-6378.

[24] S-C. Cheng, H-J. Lin, C-Y. Lee, M-Z. Huang, J. Shiea, Gas chromatography combined with flame-induced atmospheric pressure chemical ionization mass spectrometry for the analysis of fatty acid methyl esters and saturated hydrocarbons. Anal. Chim. Acta 1200 (2022) 339611.

[25] S. Mitschke, W. Welthagen, R. Zimmermann, Comprehensive gas chromatography-time-of-flight mass spectrometry using soft and selective photoionization techniques. Anal. Chem. 78 (2006) 6364−6375.

[26] JEOL, Application note, MS MSTips No. 358, GC-QMS Application.

[27] V. Schäfer, K-M. Weitzel, Qualitative and quantitative distinction of *ortho*-, *meta*-, and *para*-fluorotoluene by means of chirped femtosecond laser ionization. Anal. Chem. 92 (2020) 5492−5499.

[28] S. L. McPherson, J. M. Shusterman, H. A. López Peña, D. A. Boateng, K. M. Tibbetts, Quantitative analysis of nitrotoluene isomer mixtures using femtosecond time-resolved mass spectrometry. Anal. Chem. 93 (2021) 11268-11274.

[29] T. Imasaka, T. Imasaka, Femtosecond ionization mass spectrometry for chromatographic detection. J. Chromatogr. A, 1642 (2021) 462023.

[30] S. L. Madunil, T. Imasaka, T. Imasaka, Suppression of fragmentation in mass spectrometry. Anal. Chem. 92 (2020) 16016-16023.

[31] S. L. Madunil, T. Imasaka, T. Imasaka, Comprehensive analysis of analogues of amine-related psychoactive substances using femtosecond laser ionization mass spectrometry. Anal. Chem. 94 (2022) 14691-14698.

[32] L. Wen, K. Yoshinaga, T. Imasaka, T. Imasaka, Trace analysis of nitrated polycyclic aromatic hydrocarbons based on two-color femtosecond laser ionization mass spectrometry. Talanta 265 (2023) 124807.

[33] K. Yoshinaga, N. V. Hao, T. Imasaka, T. Imasaka, Miniature time-of-flight mass analyzer for use in combination with a compact highly-repetitive femtosecond laser ionization source. Anal. Chim. Acta 1203 (2022) 339673.

[34] R. Bauernschmitt, R. Ahlrichs, Treatment of electronic excitations within the adiabatic approximation of time dependent density functional theory. Chem. Phys. Lett. 256 (1996) 454-464.

[35] T. L. Blasbalg, J. R. Hibbeln, C. E. Ramsden, S. F. Majchrzak, R. R. Rawlings, Changes in consumption of omega-3 and omega-6 fatty acids in the United States during the 20th century. Am. J. Clin. Nutr. 93 (2011) 950-962.

[36] Z. Al-Hamamre, J. Yamin, Parametric study of the alkali catalyzed transesterification of waste frying oil for biodiesel production. Energy Convers. Manage. 79 (2014) 246-254.

[37] O. Awogbemi, E. I. Onuh, F. L. Inambao, Comparative study of properties and fatty acid composition of some neat vegetable oils and waste cooking oils. Int. J. Low Carbon Technol. 14 (2019) 417-425.

[38] A. Li, T. Imasaka, Internal standards for use in the comprehensive analysis of polychlorinated aromatic hydrocarbons using gas chromatography combined with multiphoton ionization mass spectrometry. J. Chromatogr. A 1470 (2016) 111-117.

Table 1 Signal intensities of FAMEs measured by fsLIMS, EIMS, and PIMS.

No.	Compounds	LIMS	EIMS	PIMS	Ratio A/B	Ratio A/C
		A[a)]	B[a)]	C[a)]		
23	Methyl *cis*-5,8,11,14,17-eicosapentaenoate (C20:5)	0.32	<0.005 [b)]	<0.005 [b)]	>64 [b)]	>64
24	Methyl *cis*-5,8,11,14-eicosatetraenoate (C20:4)	0.63	<0.005 [b)] 0.01 [c)]	0.024 [b)]	>130 [b)] 63 [c)]	26
25	Methyl *cis*-8,11,14-eicosatrienoate (C20:3)	1.45	0.028 [b)] 0.04 [d)]	0.55 [b)]	52 [b)] 36 [d)]	2.6
27	Methyl *cis*-11,14-eicosadienoate (C20:2)	11.9	0.042 [b)] 0.21 [d)]	1.10 [b)]	280 [b)] 57 [d)]	11
28	Methyl *cis*-11-eicosenoate (C20:1)	4.78	0.014 [b)]	0.13 [b)]	340 [b)]	37
29	Methyl arachidate (C20:0)	2.69	0.075 [b)] 0.41 [c)]	2.1 [b)]	36 [b)] 6.6 [c)]	1.3

a) A, B, and C are the ratios of the signal intensities measured for M^+ and F^+ using fsLIMS, EIMS, and PIMS, respectively. Data; a) this work, b) ref. 26, c) NIST, d) Sci. Finder.

Figure Captions

Fig. 1 Chemical structures of the FAMEs examined in this study. (A) methyl gamma-linolenate (C18:3) (B) methyl linolenate (C18:3) (C) methyl linoleate (C18:2) (D) methyl linolelaidate (C18:2) (E) methyl oleate (C18:1) (F) methyl elaidate (C18:1) (G) methyl stearate (C18:0).

Fig. 2 Experimental apparatus of GC-MS based on time-correlated single ion counting.

Fig. 3 Ionization Scheme for (A) unsaturated (B) saturated FAMEs. The numbers are the two-photon energy and the ionization energy (eV). The π-π* transition does not appear for saturated FAMEs in the data calculated by the Gaussian Program and is not shown in (B).

Fig. 4 (A) Two-dimensional GC-MS display measured for a sample mixture (ca. 400 ppm) containing 37 FAMEs. (B) Expanded views of the two-dimensional GC-MS display measured for a sample mixture containing 37 FAMEs in portion (a) C18:0 - C18:3 (b) C20:0 - C20:5 (c) C22:0 - C22:6. Ionization source, 257 nm (53 mW) + 206 nm (17 mW). The number in the figure shows the component number of the FAMEs indicated in the experimental section. The signals with no numbers appeared in the regions of ca. m/z = 290 and t_r = 21.5 and m/z = 320 and t_r = 24 do not originate from the fragment ions of FAMEs but from some unknown chemical species in the sample.

Fig. 5 Mass spectra measured for FAMEs. (A) methyl stearate (C18:0) (B) methyl oleate (C18:1) (C) methyl linoleate (C18:2) (D) methyl linolenate (C18:3) (E) methyl *cis*-11,14-eicosadienoate (C20:2) (F) methyl *cis*-5,8,11,14,17-eicosapentaenoate (C20:5) (G) methyl *cis*-4,7,10,13,16,19-docosahexaenoate (C22:6). Analytes (A) and (B) were prepared at two-times higher concentrations (4 ppm) than those (2 ppm) of (C)-(G) by the manufacturer.

Fig. 6 (A) Two-dimensional display of GC-MS measured for an actual sample of B5. (B) Expanded view of the portion indicated by a square line in (A). The number in the figure shows the component number of FAMEs indicated in the experimental section.

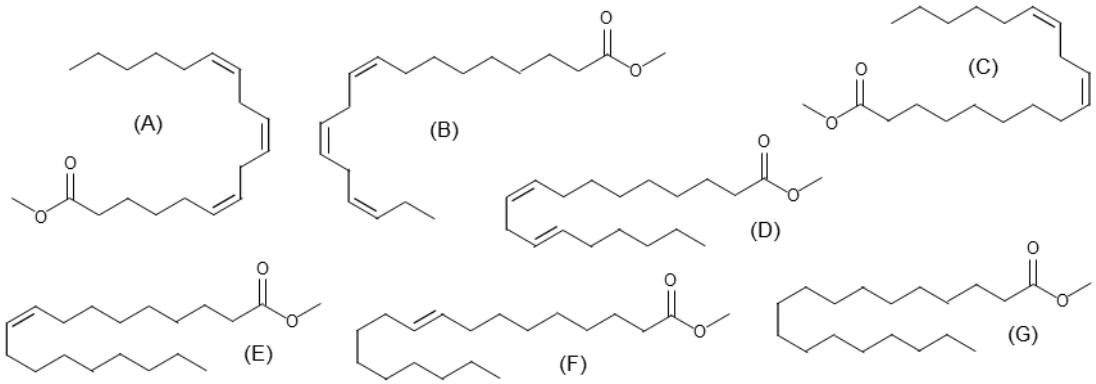

Fig. 1 K. Yoshinaga, et al.

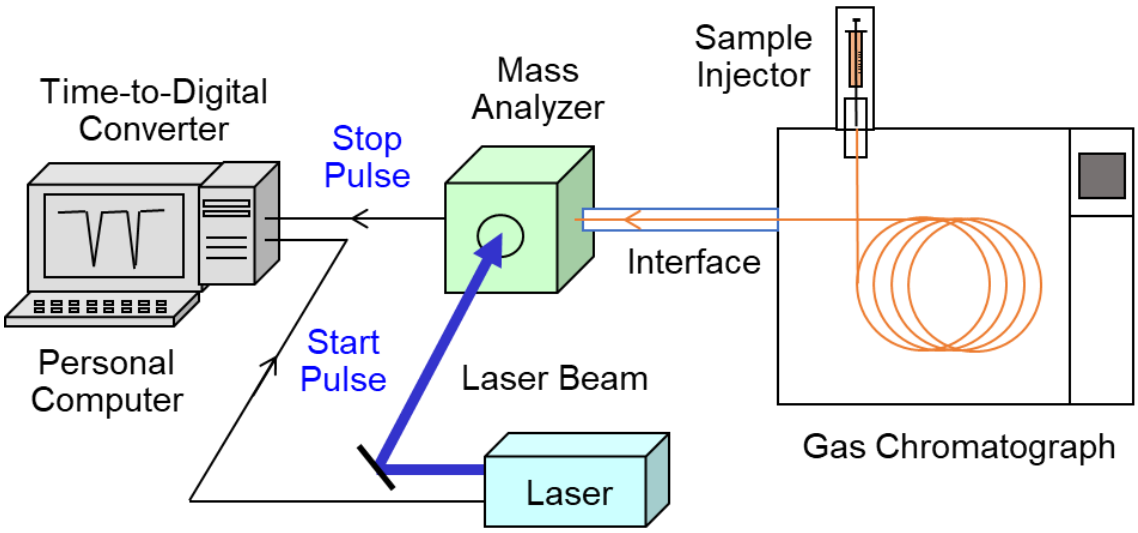

Fig. 2 K. Yoshinaga, et al.

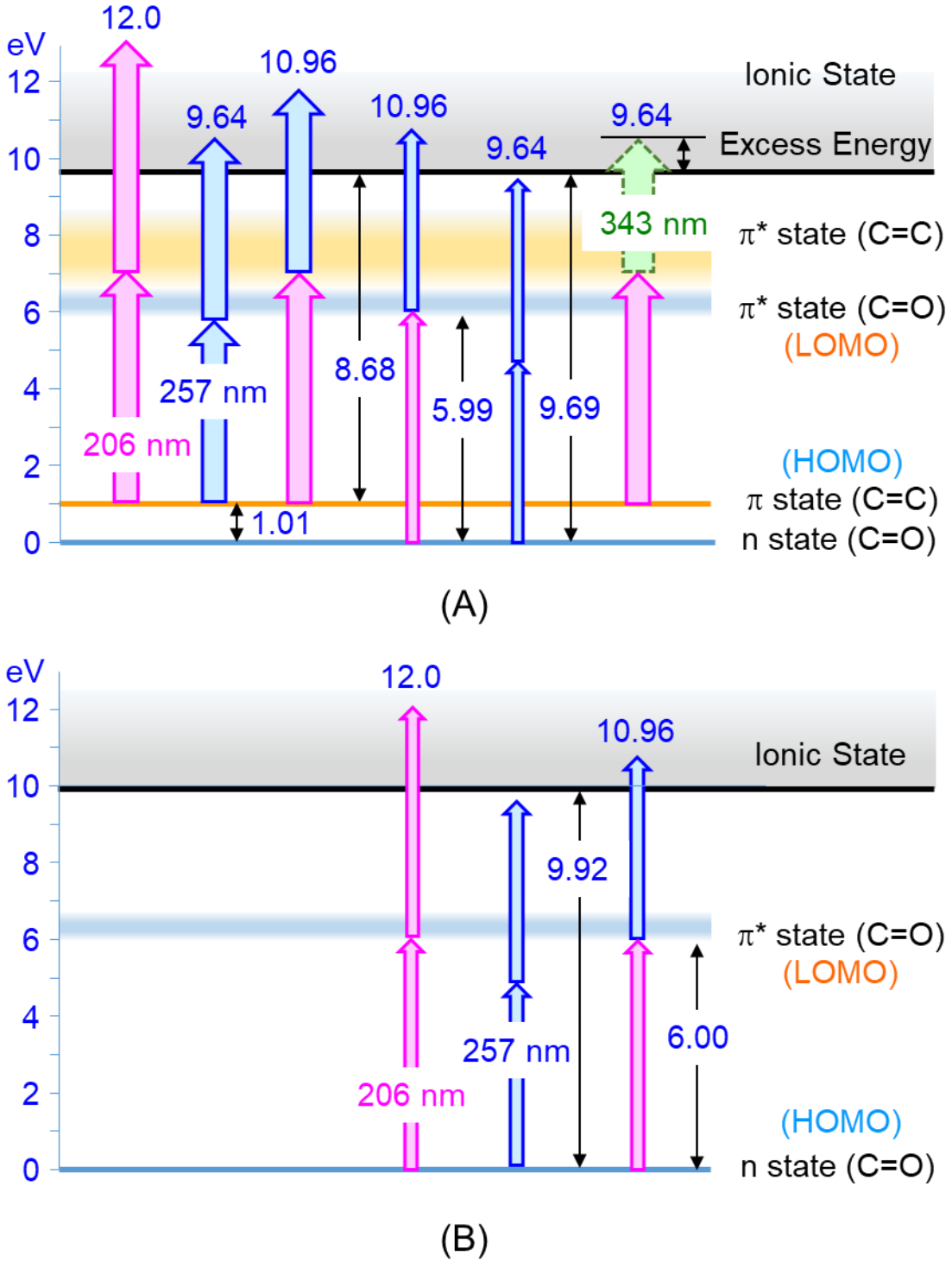

Fig. 3 K. Yoshinaga, et al.

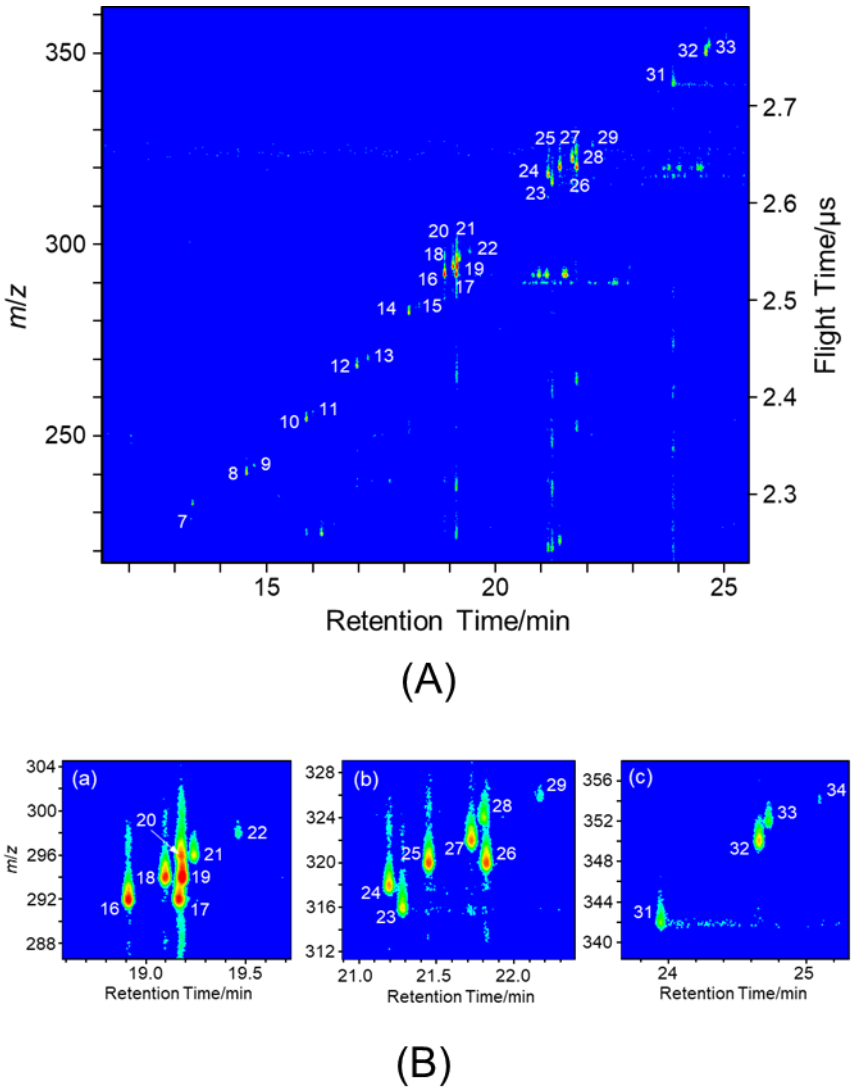

Fig. 4 K. Yoshinaga, et al.

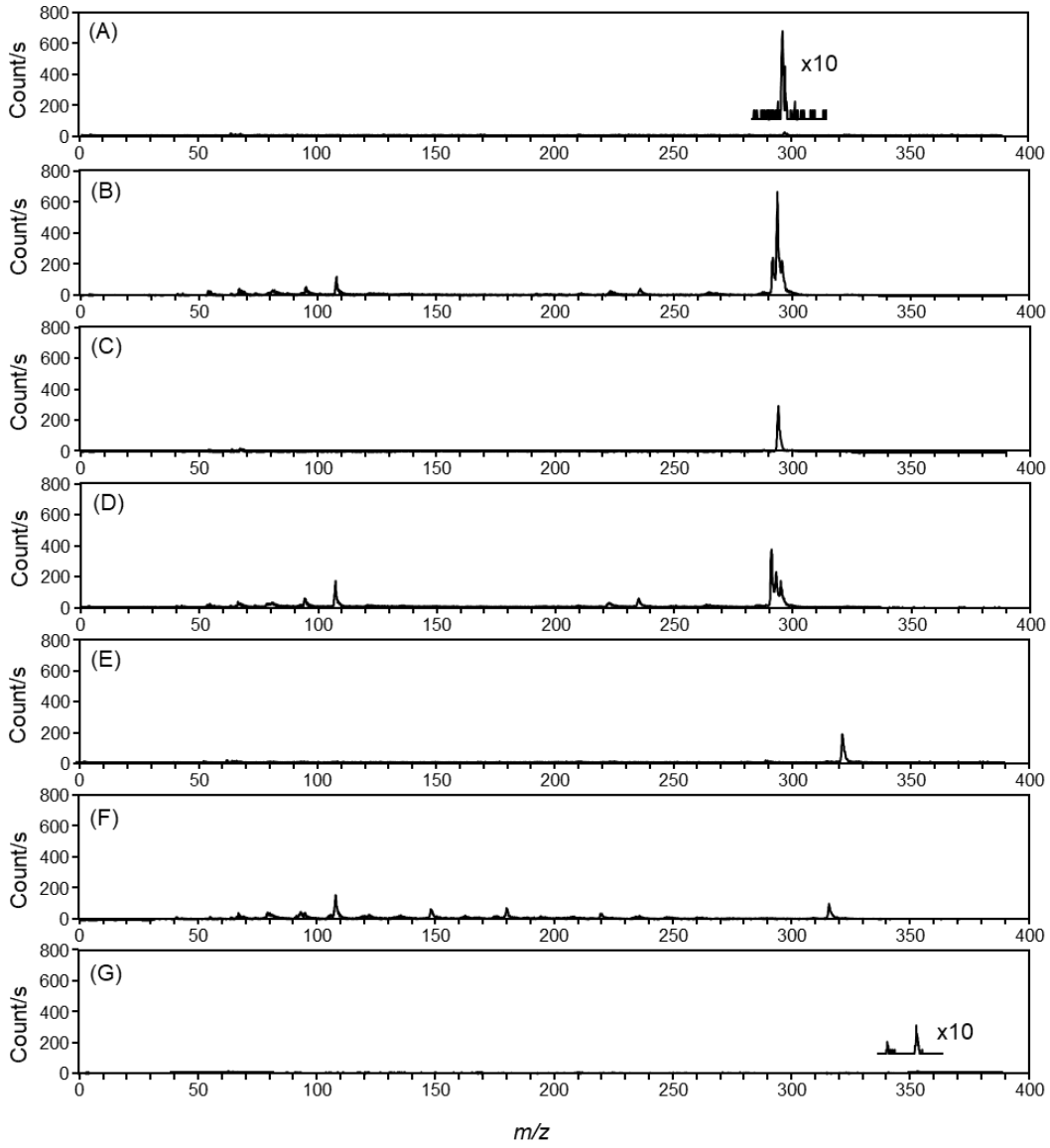

Fig. 5 K. Yoshinaga, et al.

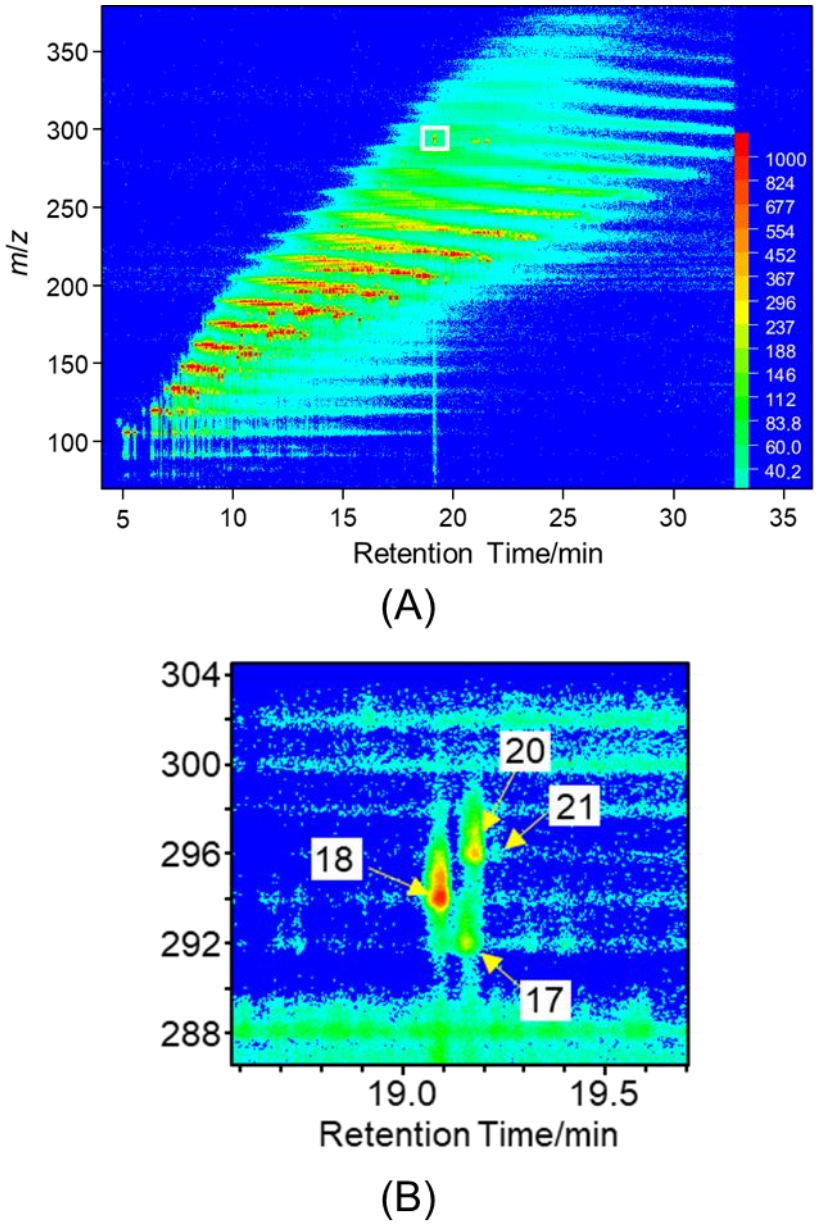

Fig. 6 K. Yoshinaga, et al.

Supplementary Information

Determination of fatty acid methyl esters by two-color two-photon resonance-enhanced femtosecond ionization mass spectrometry

Katsunori Yoshinaga,[a,1] Lu Wen,[a,1,2] Totaro Imasaka,[b,c] and Tomoko Imasaka[a]*

[a]*Faculty of Design, Kyushu University, 4-9-1, Shiobaru, Minami-ku, Fukuoka 815-8540: 744 Motooka, Nishi-ku, Fukuoka 819-0395, Japan*

[b]*Kyushu University, 744 Motooka, Nishi-ku, Fukuoka 819-0395, Japan*

[c]*Hikari Giken, Co., 2-10-30, Sakurazaka, Chuou-ku, Fukuoka 810-0024, Japan*

* Corresponding author.

Email address: imasaka@design.kyushu-u.ac.jp (Tomoko Imasaka).

1. These authors have contributed equally to this work.

2. Present address: Shijiazhuang University, No.288, Zhufeng street, Shijiazhuang high tech Development Zone, China.

Table of contents:

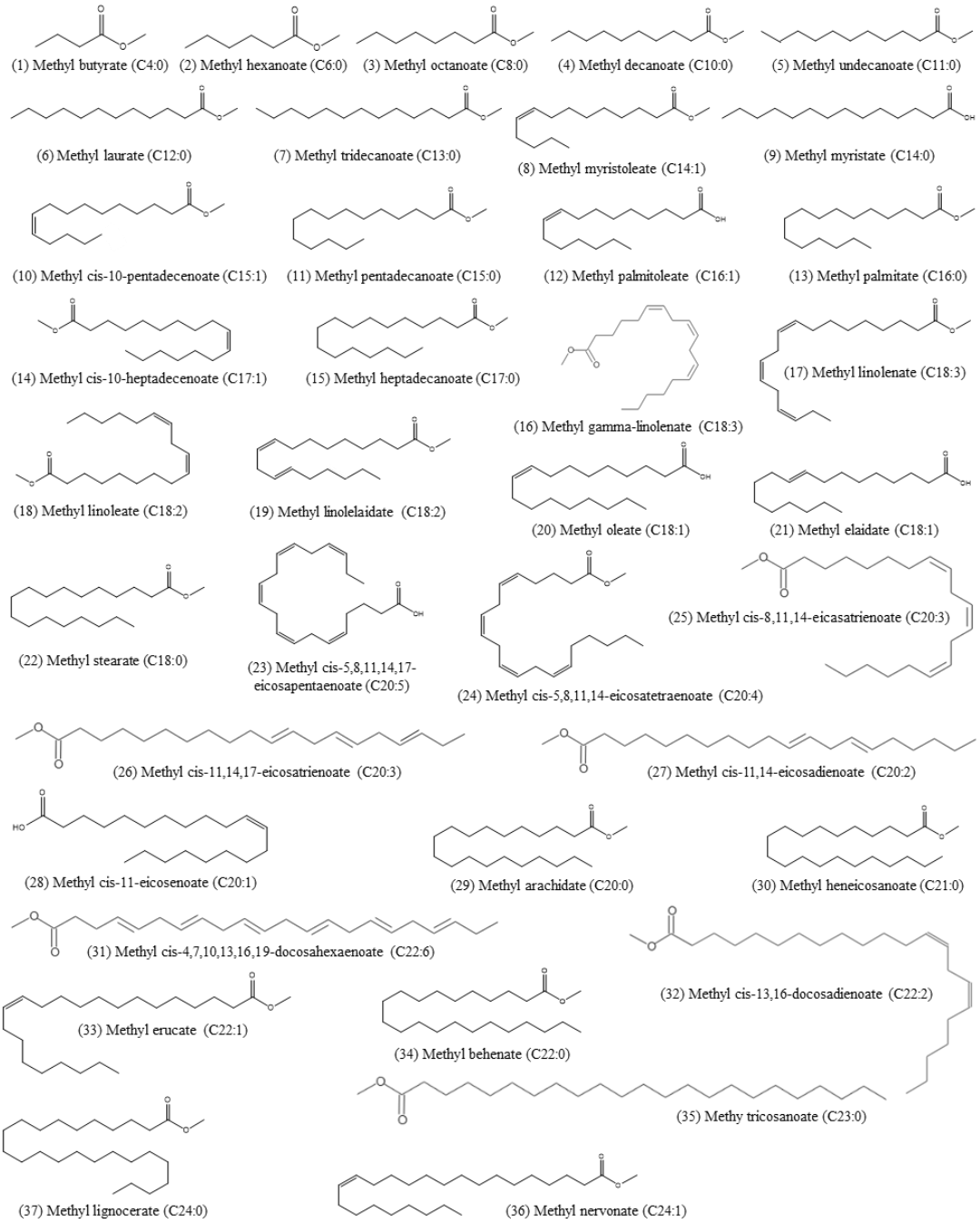

Figure S1. Chemical structures of the FAMEs measured in this study.

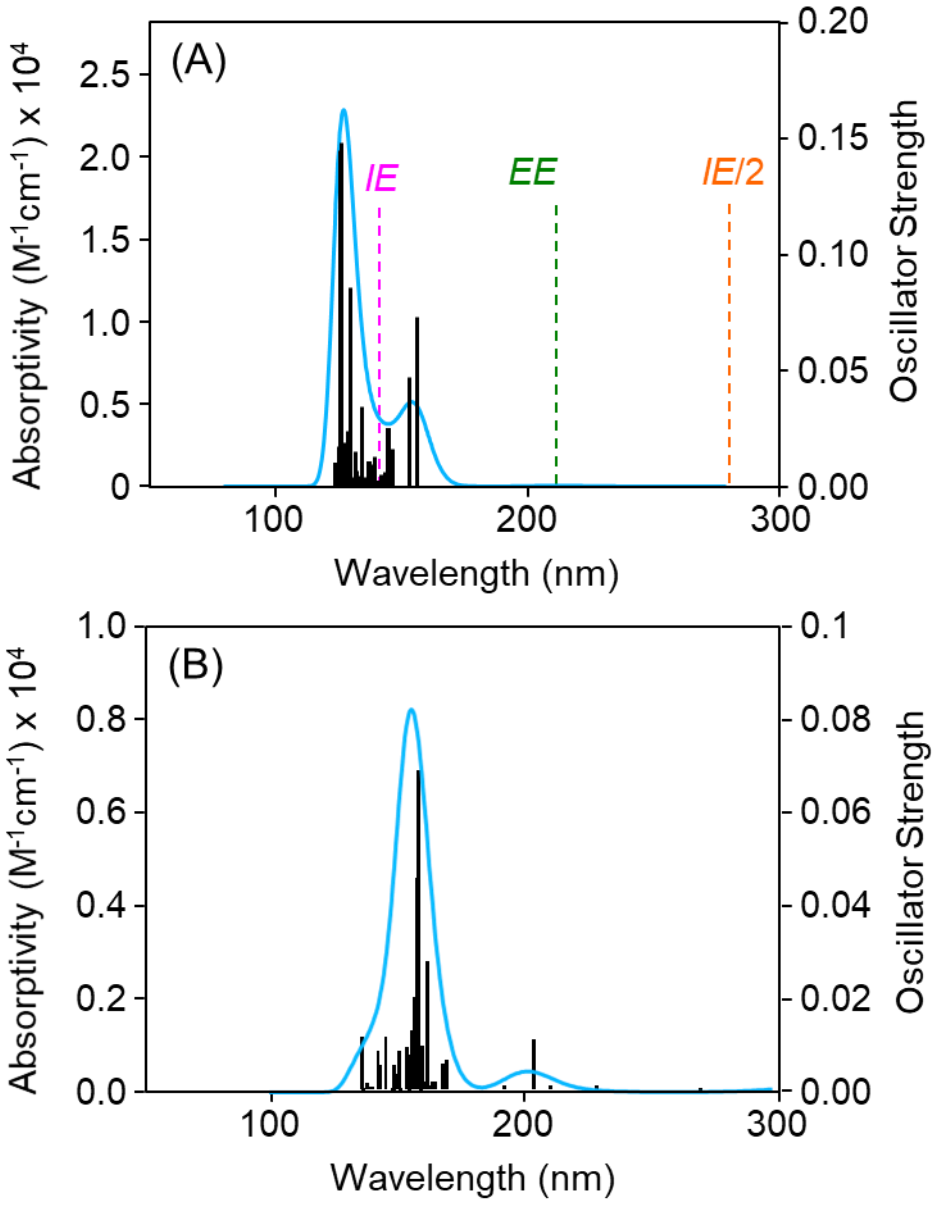
(A)
IE
EE
IE/2
Absorptivity (M-1cm-1) x 10^4
Oscillator Strength
Wavelength (nm)
(B)
Absorptivity (M-1cm-1) x 10^4
Oscillator Strength
Wavelength (nm)

(1)

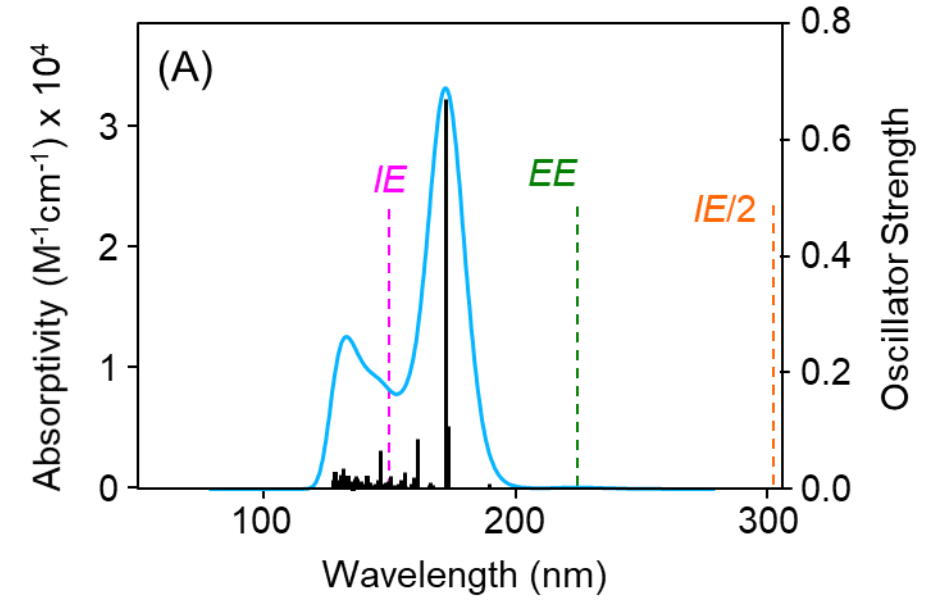
(A)
IE
EE
IE/2
Absorptivity (M-1cm-1) x 10^4
Oscillator Strength
Wavelength (nm)
0
1
2
3
0.0
0.2
0.4
0.6
0.8
100
200
300

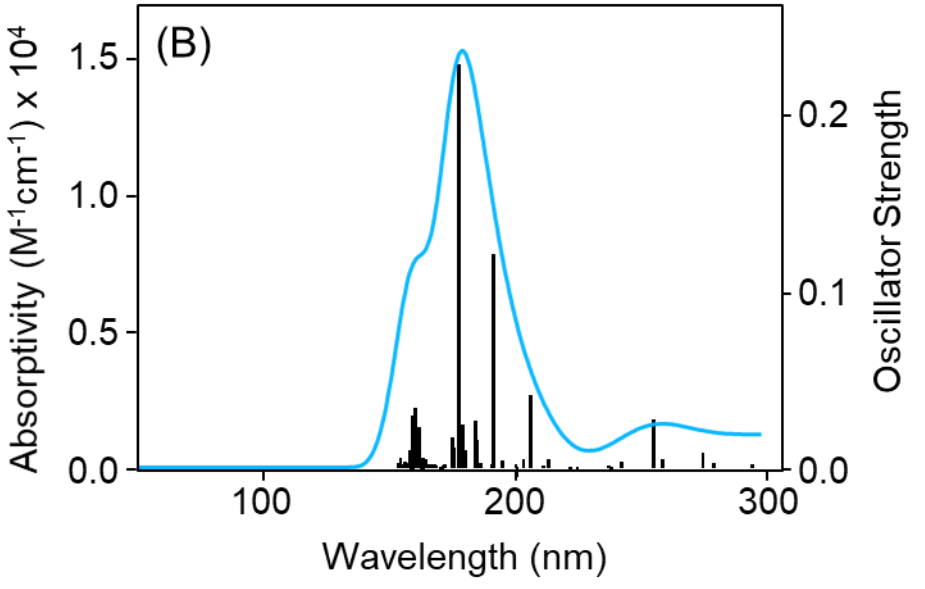
(B)
Absorptivity (M-1cm-1) x 10^4
Oscillator Strength
Wavelength (nm)
0.0
0.5
1.0
1.5
0.0
0.1
0.2
100
200
300

(2)

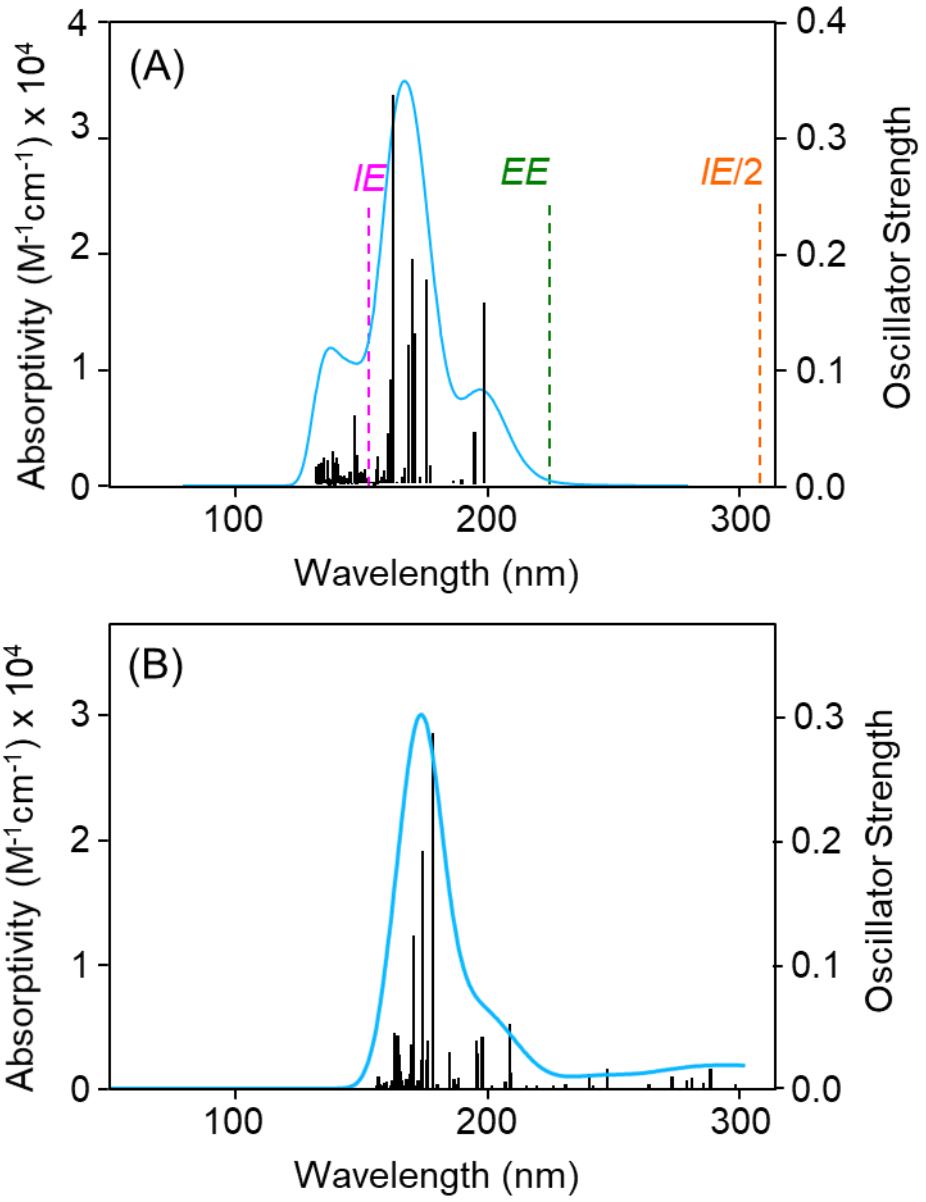
(A)
IE
EE
IE/2
Absorptivity (M-1cm-1) x 10^4
Oscillator Strength
Wavelength (nm)
(B)
Absorptivity (M-1cm-1) x 10^4
Oscillator Strength
Wavelength (nm)

(3)

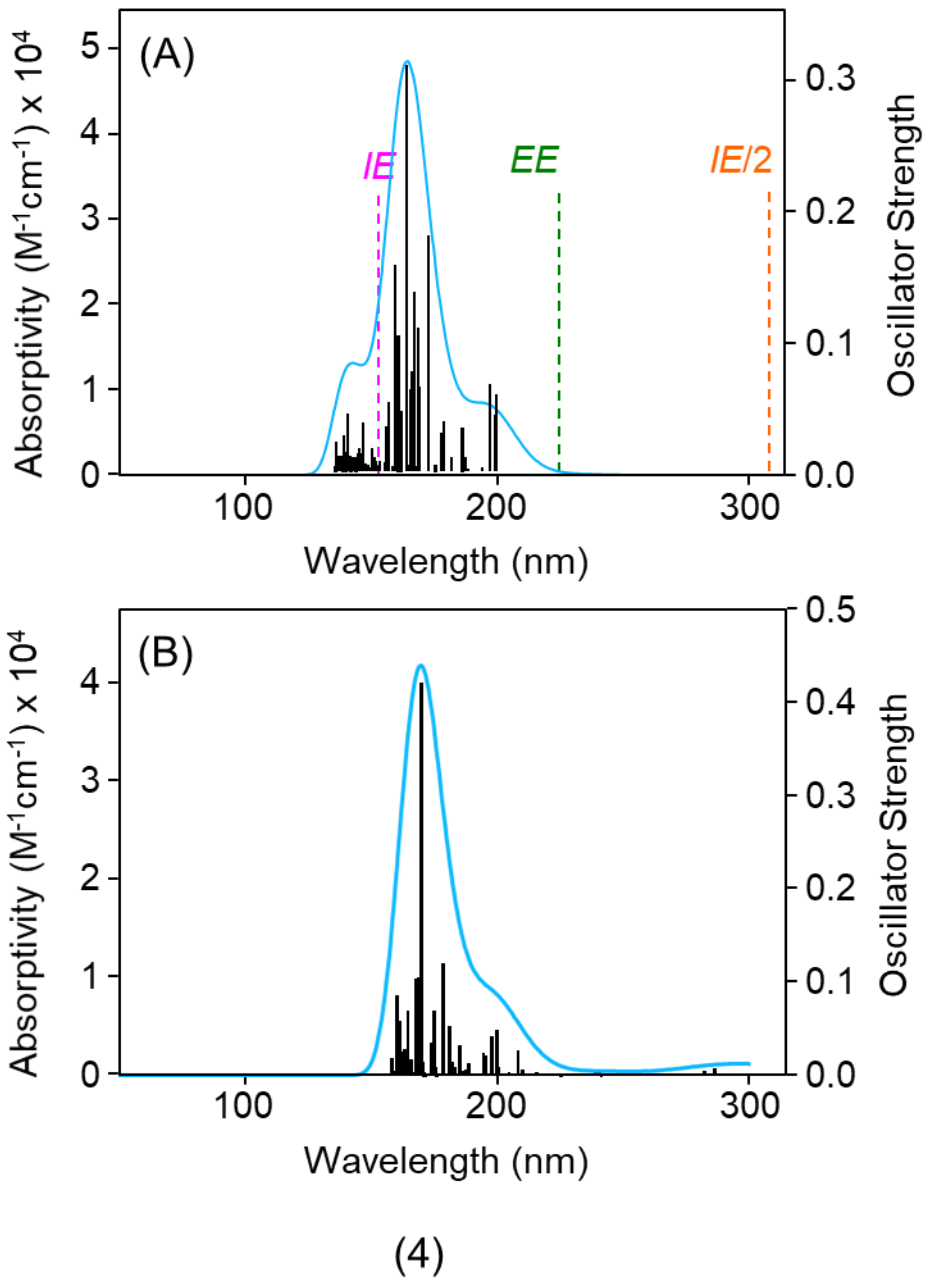

Figure S2. Calculated absorption spectra for (1) stearic (2) oleic (3) linoleic (4) linolenic FAMEs for (A) neutral and (B) ionic species. The wavelengths corresponding to the first excited energy (*EE*), the ionization energy (*IE*), and the half value of the ionization energy (*IE*/2) are indicated in the figure.

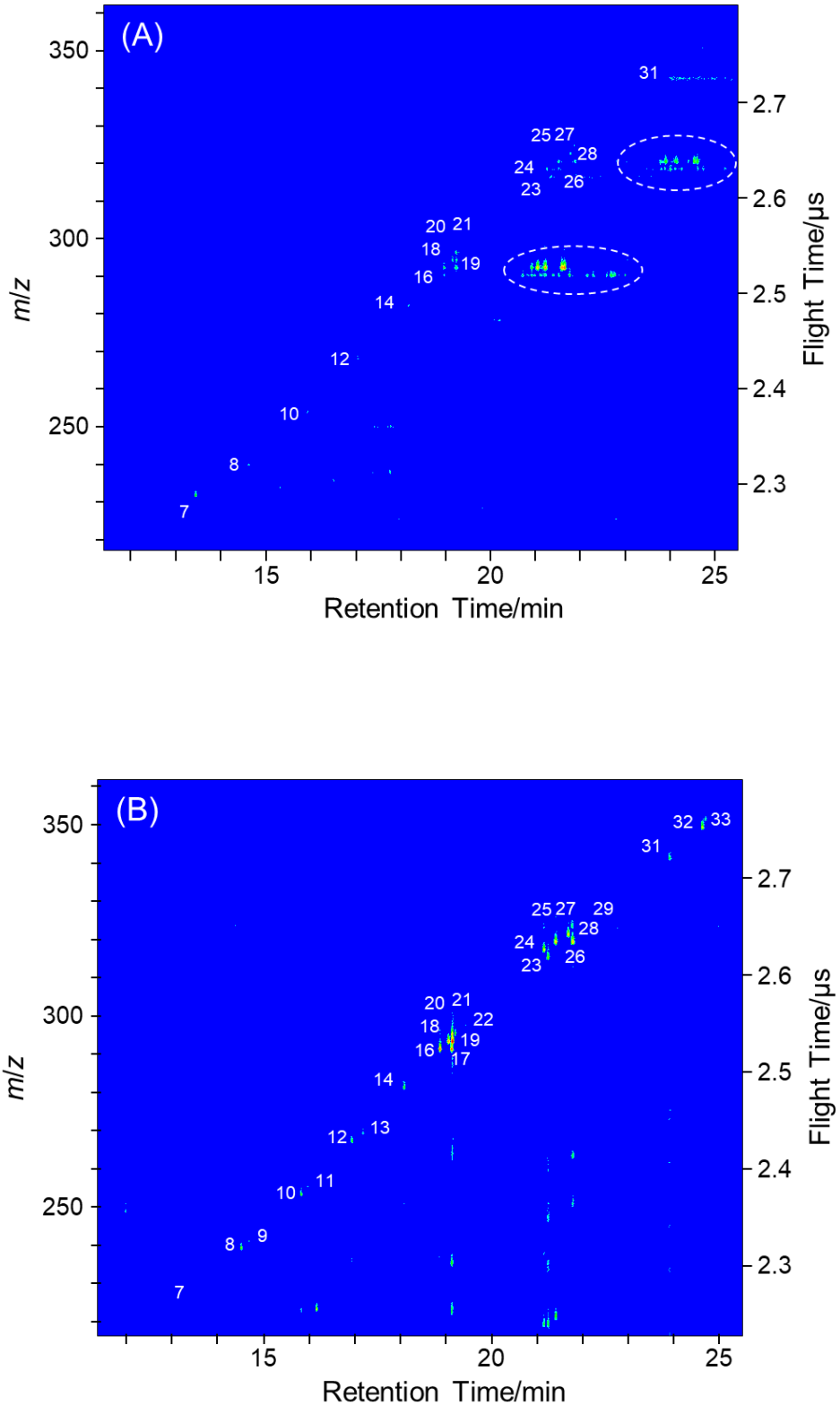

Figure S3. Two-dimensional display of GC-MS measured for a sample mixture (ca. 400 ppm) containing 37 FAMEs at (A) 257 nm, 53 mW (B) 206 nm, 17.3 mW.

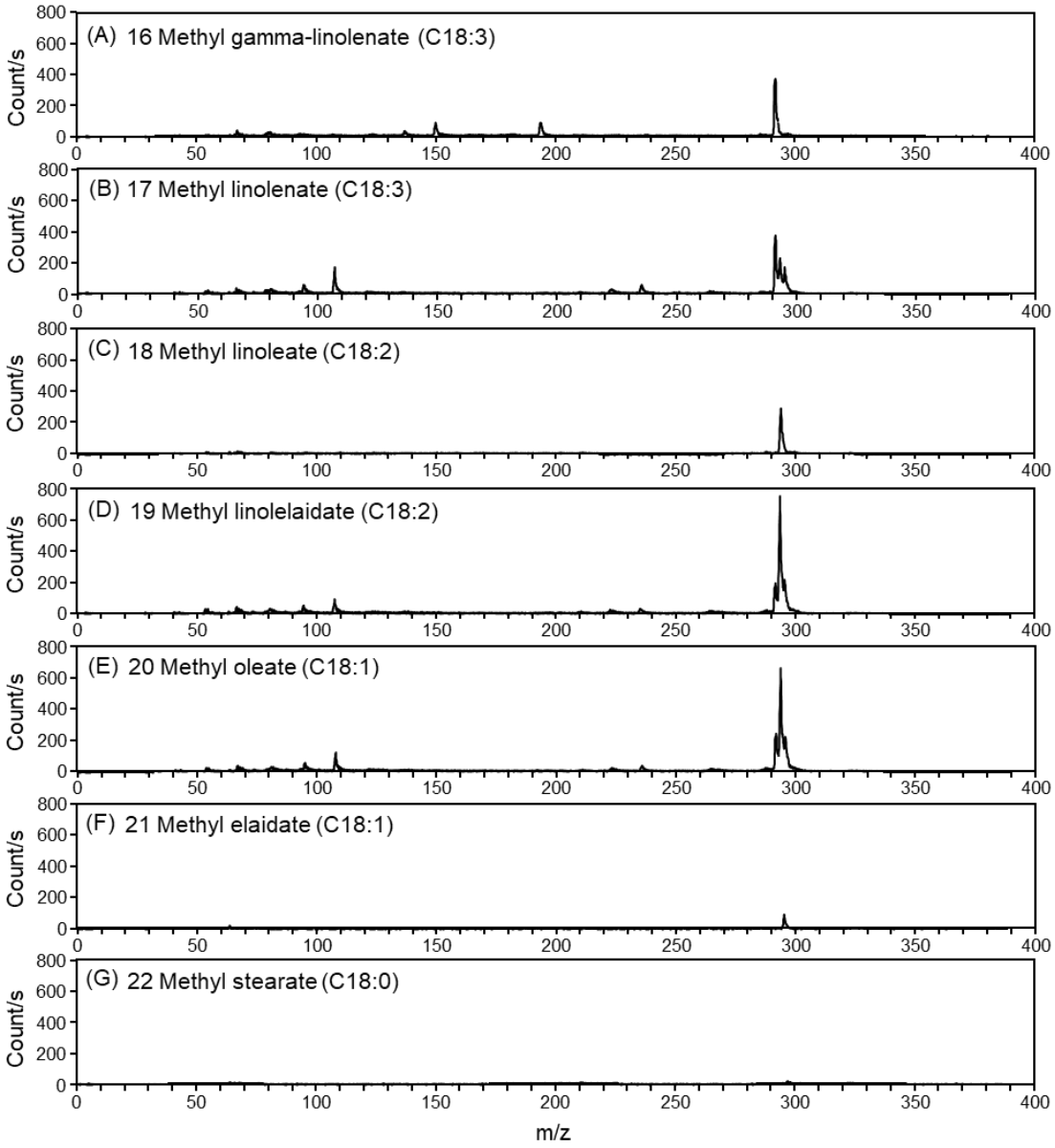
(A) 16 Methyl gamma-linolenate (C18:3)
(B) 17 Methyl linolenate (C18:3)
(C) 18 Methyl linoleate (C18:2)
(D) 19 Methyl linolelaidate (C18:2)
(E) 20 Methyl oleate (C18:1)
(F) 21 Methyl elaidate (C18:1)
(G) 22 Methyl stearate (C18:0)
Count/s
m/z

(1)

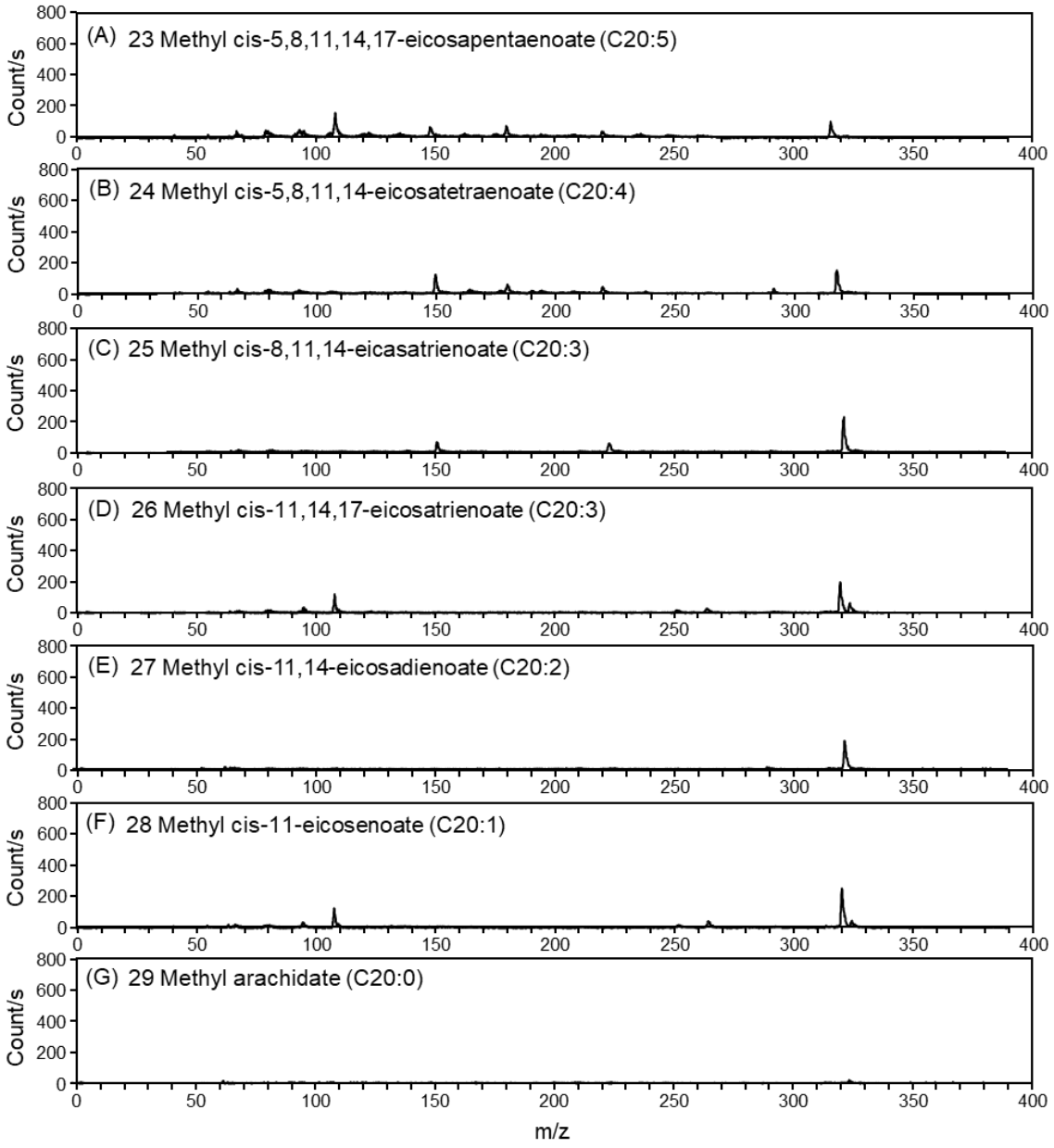
(A) 23 Methyl cis-5,8,11,14,17-eicosapentaenoate (C20:5)
(B) 24 Methyl cis-5,8,11,14-eicosatetraenoate (C20:4)
(C) 25 Methyl cis-8,11,14-eicasatrienoate (C20:3)
(D) 26 Methyl cis-11,14,17-eicosatrienoate (C20:3)
(E) 27 Methyl cis-11,14-eicosadienoate (C20:2)
(F) 28 Methyl cis-11-eicosenoate (C20:1)
(G) 29 Methyl arachidate (C20:0)
Count/s
m/z

(2)

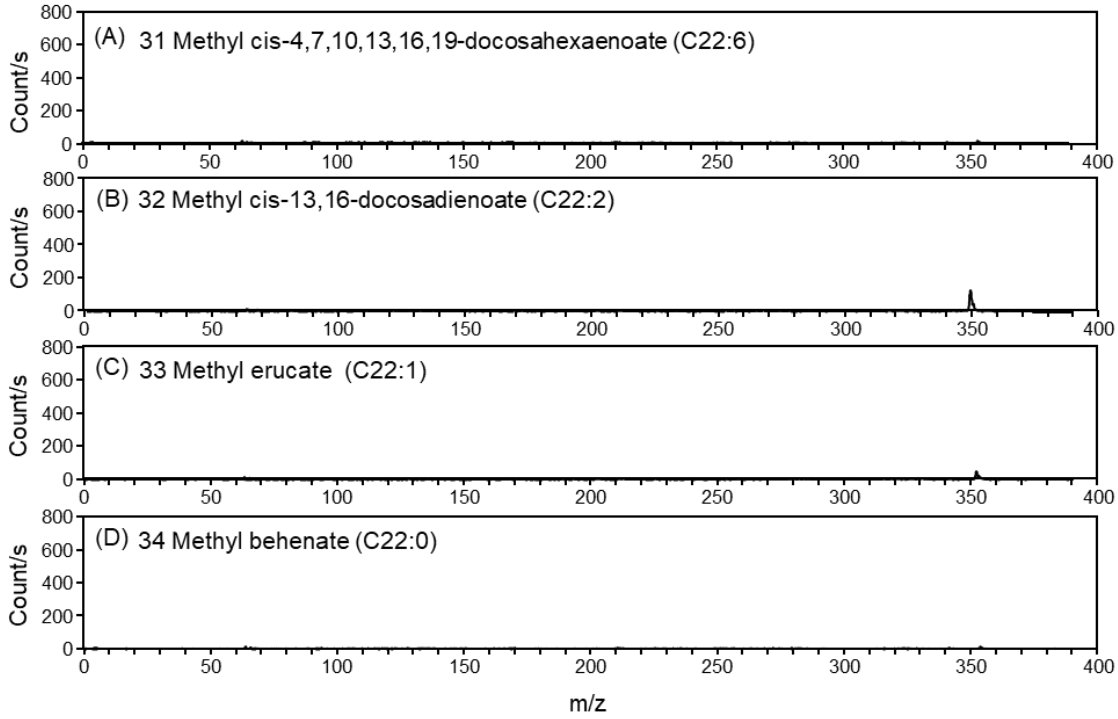

(3)

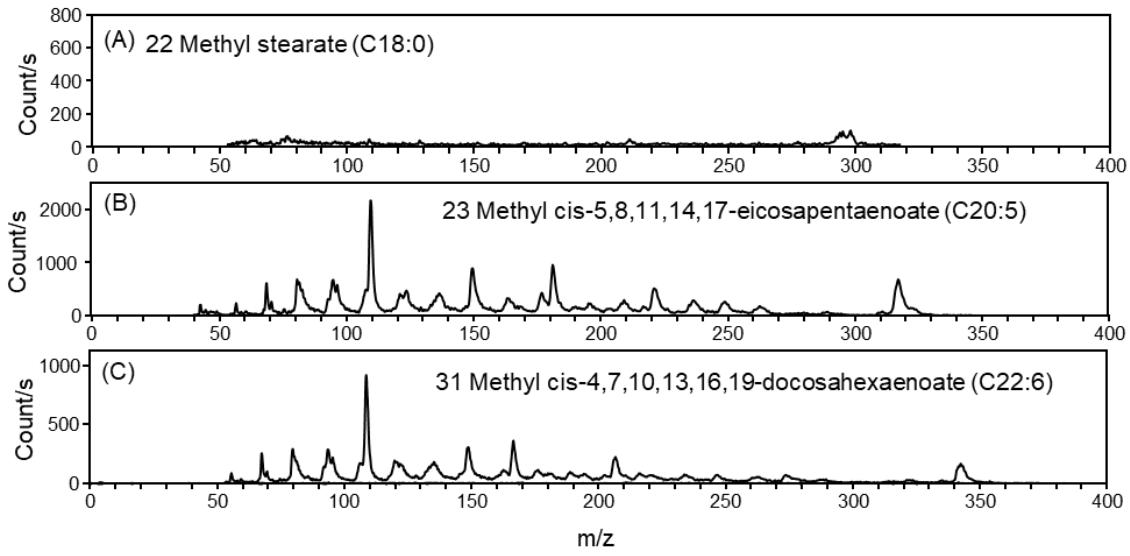

(4)

Figure S4. Mass spectra for (1) C18:0-3 (2) C20:0-5 (3) C22:0-6. (4)C18:0, C20:5, C22:6 (the data measured at high sensitivity). The name of the compound is indicated in the figure.

Table S1. Properties of FAMEs and the excitation and ionization energies calculated in this study.

Elution time	Compounds	CAS	M.W.	Formula	*EE*[a)]	*IE*[a)]
1	Methyl butyrate (C4:0)	623-42-7	102.13	$C_5H_{10}O_2$	-	-
2	Methyl hexanoate (C6:0)	106-70-7	130.18	$C_7H_{14}O_2$	-	-
3	Methyl octanoate (C8:0)	111-11-5	158.24	$C_9H_{18}O_2$	-	-
4	Methyl decanoate (C10:0)	110-42-9	186.29	$C_{11}H_{22}O_2$	-	-
5	Methyl undecanoate (C11:0)	1731-86-8	200.32	$C_{12}H_{24}O_2$	-	-
6	Methyl laurate (C12:0)	111-82-0	214.34	$C_{13}H_{26}O_2$	-	-
7	Methyl tridecanoate (C13:0)	1731-88-0	228.37	$C_{14}H_{28}O_2$	-	-
8	Methyl myristoleate (C14:1)	56219-06-8	240.38	$C_{15}H_{28}O_2$	-	-
9	Methyl myristate (C14:0)	124-10-7	242.40	$C_{15}H_{30}O_2$	-	-
10	Methyl cis-10-pentadecenoate (C15:1)	90176-52-6	254.41	$C_{16}H_{30}O_2$	-	-
11	Methyl pentadecanoate (C15:0)	7132-64-1	256.42	$C_{16}H_{32}O_2$	-	-
12	Methyl palmitoleate (C16:1)	1120-25-8	268.43	$C_{17}H_{32}O_2$	5.99	8.69
13	Methyl palmitate (C16:0)	112-39-0	270.45	$C_{17}H_{34}O_2$	5.89	9.84
14	Methyl cis-10-heptadecenoate (C17:1)	75190-82-8	282.46	$C_{18}H_{34}O_2$	-	-
15	Methyl heptadecanoate (C17:0)	1731-92-6	284.48	$C_{18}H_{36}O_2$	-	-
16	Methyl gamma-linolenate (C18:3)	16326-32-2	292.5	$C_{19}H_{32}O_2$	6.00	8.49
17	Methyl linolenate (C18:3) cis-9-12-15	301-00-8	292.46	$C_{19}H_{32}O_2$	6.00	8.45
18	Methyl linoleate (C18:2)	112-63-0	294.47	$C_{19}H_{34}O_2$	5.99	8.50
19	Methyl linolelaidate (C18:2)	2566-97-4	294.47	$C_{19}H_{34}O_2$	5.99	8.60
20	Methyl oleate (C18:1)	112-62-9	296.49	$C_{19}H_{36}O_2$	5.99	8.68
21	Methyl elaidate (C18:1)	1937-62-8	296.49	$C_{19}H_{36}O_2$	6.00	8.69
22	Methyl stearate (C18:0)	112-61-8	298.50	$C_{19}H_{38}O_2$	6.00	9.92
23	Methyl cis-5,8,11,14,17-eicosapentaenoate (C20:5)	2734-47-6	316.48	$C_{21}H_{32}O_2$	5.85	8.24
24	Methyl cis-5,8,11,14-eicosatetraenoate (C20:4)	2566-89-4	318.49	$C_{21}H_{34}O_2$	5.98	8.54
25	Methyl cis-8,11,14-eicasatrienoate (C20:3)	21061-10-9	320.5	$C_{21}H_{36}O_2$	6.00	8.70
26	Methyl cis-11,14,17-eicosatrienoate (C20:3)	55682-88-7	320.5	$C_{21}H_{36}O_2$	6.00	8.68
27	Methyl cis-11,14-eicosadienoate (C20:2)	61012-46-2	322.52	$C_{21}H_{38}O_2$	6.00	8.50
28	Methyl cis-11-eicosenoate (C20:1)	2390-09-2	324.54	$C_{21}H_{40}O_2$	5.99	8.67
29	Methyl arachidate (C20:0)	1120-28-1	326.56	$C_{21}H_{42}O_2$	5.99	9.89
30	Methyl heneicosanoate (C21:0)	6064-90-0	340.58	$C_{22}H_{44}O_2$	-	-
31	Methyl cis-4,7,10,13,16,19-docosahexaenoate (C22:6)	2566-90-7	342.51	$C_{23}H_{34}O_2$	5.94	8.42
32	Methyl cis-13,16-docosadienoate (C22:2)	61012-47-3	350.58	$C_{23}H_{42}O_2$	5.99	8.49
33	Methyl erucate (C22:1)	1120-34-9	352.59	$C_{23}H_{44}O_2$	5.99	8.66
34	Methyl behenate (C22:0)	929-77-1	354.61	$C_{23}H_{46}O_2$	6.00	9.87
35	Methyl tricosanoate (C23:0)	2433-97-8	368.64	$C_{24}H_{48}O_2$	-	-
36	Methyl nervonate (C24:1)	2733-88-2	380.65	$C_{25}H_{48}O_2$	-	-
37	Methyl lignocerate (C24:0)	2442-49-1	382.66	$C_{25}H_{50}O_2$	-	-

a) The values were calculated only for important FAMEs, since it typically takes a few days for calculating these parameters for one compound.

Table S2. Signal intensities measured by fs-LIMS and EIMS.

No.	Analyte	Conc (%)	Symbol	Mw	LIMS				EIMS		Ratio A/B
					M^+	$F^{+a)}$	$m/z^{b)}$	$A^{c)}$	$B^{c)}$	$m/z^{b)}$	
1	Methyl butyrate	3.4	C4:0	102	-	-	-	-	0.03	43	-
2	Methyl hexanoate	4	C6:0	130	13	199	74	0.065	0.01	74	6.5
3	Methyl octanoate	4	C8:0	158	35	341	74	0.10	0.04	74	2.6
4	Methyl decanoate	4	C10:0	186	57	226	74	0.25	0.03	74	8.4
5	Methyl undecanoate	2	C11:0	200	34	92	74	0.37	0.04	74	9.2
6	Methyl laurate	4	C12:0	214	38	113	74	0.34	0.07	74	4.8
7	Methyl tridecanoate	2	C13:0	228	35	59	74	0.59	0.04	74	15
8	Methyl myristoleate	2	C14:1	240	611	69	210	8.86	0.05	55	180
9	Methyl myristate	4	C14:0	242	73	41	75	1.78	0.06	74	30
10	Methyl cis-10-pentadecenoate	2	C15:1	254	506	129	223	3.92	0.07	55	56
11	Methyl pentadecanoate	2	C15:0	256	53	91	224	0.58	0.06	74	9.7
12	Methyl palmitoleate	2	C16:1	268	392	95	238	4.13	0.07	55	59
13	Methyl palmitate	6	C16:0	270	84	84	75	1.00	0.09	74	11
14	Methyl cis-10-heptadecenoate	2	C17:1	282	378	99	251	3.82	<0.005	55	>760
15	Methyl heptadecanoate	2	C17:0	284	54	63	76	0.86	0.08	74	11
16	Methyl gamma-linolenate	2	C18:3	292	1558	872	150	1.79	0.08	79	22
17	Methyl linolenate	2	C18:3	292	953	975	108	0.98	0.07	79	14
18	Methyl linoleate	2	C18:2	294	797	90	67	8.86	0.20	67	44
19	Methyl linolelaidate	2	C18:2	294	3840	371	67	10.35	0.30	67	35
20	Methyl oleate	4	C18:1	296	489	45	225	10.87	0.07	55	160
21	Methyl elaidate	2	C18:1	296	520	94	265	5.53	0.09	55	61
22	Methyl stearate	4	C18:0	298	76	<5	-	>15	0.15	74	>100
23	Methyl cis-5,8,11,14,17-eicosapentaenoate	2	C20:5	316	682	2116	108	0.32	<0.005	79	>64
24	Methyl cis-5,8,11,14-eicosatetraenoate	2	C20:4	318	624	988	150	0.63	0.01	79	63
25	Methyl cis-8,11,14-eicosatrienoate	2	C20:3	320	1178	812	150	1.45	0.04	43	36
26	Methyl cis-11,14,17-eicosatrienoate	2	C20:3	320	919	969	108	0.95	0.09	79	11
27	Methyl cis-11,14-eicosadienoate	2	C20:2	322	736	62	67	11.87	0.21	67	57
28	Methyl cis-11-eicosenoate	2	C20:1	324	368	77	292	4.78	0.014	55	340
29	Methyl arachidate	4	C20:0	326	78	29	79	2.69	0.41	74	6.6
30	Methyl heneicosanoate	2	C21:0	340	34	29	76	1.17	0.20	74	5.9
31	Methyl cis-4,7,10,13,16,19-docosahexaenoate	2	C22:6	342	321	1786	108	0.18	<0.005	79	>36
32	Methyl cis-13,16-docosadienoate	2	C22:2	350	586	40	110	14.65	0.14	67	100
33	Methyl erucate	2	C22:1	352	156	33	76	4.73	0.08	55	59
34	Methyl behenate	4	C22:0	354	36	21	57	1.71	0.18	74	9.5
35	Methyl tricosanoate	2	C23:0	368	15	<5	-	>3	0.18	74	>17
36	Methyl nervonate	2	C24:1	380	63	22	350	2.86	0.18	55	16
37	Methyl lignocerate	4	C24:0	382	15	<5	-	>3	0.16	74	>19

a) the signal intensity for the largest F^+ ion: b) the *m/z* value for the largest F^+ ion: c) A and B are the ratio of the signal intensities measured for M^+ and F^+ in fs-LIMS and EIMS, respectively. The concentrations (Conc) of the FAMEs in the original sample solution are indicated in the table.